

## Article

# Performance Evaluation of Asphalt Concrete Incorporating Steel Slag Powder as Filler under the Combined Damage of Temperature and Moisture

Shiquan Liu <sup>1,\*</sup>, Zhipeng Zhang <sup>1</sup> and Ruiyang Wang <sup>2</sup>

<sup>1</sup> Inner Mongolia Communications Design and Research Institute Co., Ltd., Hohhot 010000, China; zzptlw@126.com

<sup>2</sup> School of Materials Science and Engineering, Chang'an University, Xi'an 710061, China; wangruiyang@chd.edu.cn

\* Correspondence: shiquanliu@163.com; Tel.: +86-29-82337340

**Abstract:** Recycling steel slag into asphalt concrete is an important way to save natural resources and protect the environment. The high asphalt absorption and adsorption and the sensitivity of steel slag aggregate (SSA) to the combined damage of temperature and moisture (volume expansion and poor durability under freeze-thaw cycle damage) still pose risks for the use of SSA in asphalt concrete. It is urgent to develop new utilization methods of steel slag. With this in mind, the material properties of steel slag powder (SSP) and performance characteristics of asphalt concrete incorporating SSP filler were evaluated in this research. The SSP was prepared in the laboratory by grinding steel slag with a particle size of 2.36–4.75 mm. Firstly, the material properties of SSP including the specific surface area, particle gradation, apparent density, chemical compositions, and thermal stability were analyzed. Steel slag (2.36–4.75 mm) and common limestone powder (LP) filler were used as control groups. The grindability of steel slag and the advantages of using SSP as a filler in asphalt concrete were preliminarily analyzed based on the test results of material properties. Then, the Superpave method was used to design asphalt concrete incorporating SSP and LP. Considering that steel slag is sensitive to the combined damage of temperature and moisture, the main engineering performance of asphalt concrete after the combined damage of temperature and moisture was evaluated to further reveal the feasibility of using SSP as a filler. Two combined damage modes, namely hot water damage and freeze-thaw cycle damage, were applied. Results suggest that although the steel slag is more difficult to grind compared to limestone particles, grinding steel slag into SSP has improved the uniformity of its material properties. Good uniformity of material properties, high alkalinity, and excellent thermal stability of SSP give it some advantages in its application in asphalt concrete. Although the freeze-thaw cycle damage has a slightly more significant effect on the engineering performance of asphalt concrete than hot water damage, compared to the asphalt concrete with LP filler, even after freeze-thaw cycle damage for three cycles asphalt concrete incorporating SSP still possesses comparable or better volume stability, mechanical performance, high-temperature deformation resistance, low-temperature crack resistance, fatigue crack resistance, and fatigue durability.

**Keywords:** asphalt concrete; mineral filler; steel slag powder; materials property; moisture; temperature; engineering performance



**Citation:** Liu, S.; Zhang, Z.; Wang, R. Performance Evaluation of Asphalt Concrete Incorporating Steel Slag Powder as Filler under the Combined Damage of Temperature and Moisture. *Sustainability* **2023**, *15*, 14653. <https://doi.org/10.3390/su151914653>

Academic Editors: Yue Xiao, Denis Jelagin, Zongwu Chen and Dae-Wook Park

Received: 3 August 2023

Revised: 1 October 2023

Accepted: 8 October 2023

Published: 9 October 2023



**Copyright:** © 2023 by the authors. Licensee MDPI, Basel, Switzerland. This article is an open access article distributed under the terms and conditions of the Creative Commons Attribution (CC BY) license (<https://creativecommons.org/licenses/by/4.0/>).

## 1. Introduction

In the past few decades, the rapid construction of roads has significantly promoted the development of the national economy and brought great convenience to people's daily travel in China. But at the same time, the road construction consumes a large amount of natural resources. Recycling some solid waste into the construction of roads is a promising way to save natural resources and eliminate the environmental pollution caused by the

waste. Typical wastes mainly include rubber [1,2], smelting slags [3–7], construction waste [8,9], reclaimed asphalt pavement (RAP) [10,11], plastic [12,13], glass [14,15], etc.

Steel slag is one of the main smelting slags and it is produced during the steelmaking process [16]. The annual production of steel slag approaches 100 million tons in China. The efficient disposal of steel slag has always been a challenge faced by the steel industry. In recent decades, steel slag has been applied in many fields, mainly involving wastewater purification [17], sewage sludge stabilization [18,19], carbon sequestration [20,21], agriculture utilization [22], cement and concrete production [23,24], road construction [25,26], etc. Recycling steel slag in road construction is very attractive as the high consumption of materials in road construction can accelerate the disposal of solid waste. Using steel slag to replace partial natural aggregate to prepare road paving materials is one of the hot research topics [27,28]. Although many research results have proved that steel slag aggregate (SSA) can improve the skid resistance [29], high-temperature deformation resistance [30], fatigue durability [31], etc., the high asphalt content and unstable performance under the moisture damage of asphalt concrete incorporating SSA still hinder the use of SSA. These problems are mainly caused by the porous structure and active mineral compositions of SSA.

Steel slag is reported to be a porous material [32]. The porous structure results in strong absorption of liquid asphalt binder, especially for the steel slag fine aggregate (SSFA); its asphalt adsorption is also obvious due to the contribution of the powder part in the fine aggregate. Therefore, steel slag coarse aggregate (SSCA) is not suggested to be used together with the SSFA [27]. Although steel slag shows excellent adhesive performance with asphalt [33], the feedback of asphalt concrete incorporating SSA is very complex when subjected to moisture damage conditions, especially the combined damage conditions of temperature and moisture. Steel slag contains some active minerals (free lime, f-CaO, and free magnesium oxide, f-MgO). These minerals will cause volume expansion in the local zones of SSA under humid conditions after reacting with water which would bring damage to the SSA-based engineering, such as random cracking of the road surface [34]. Weathering treatment, placing steel slag in the natural environment to make the active minerals react with water before it is used, is a common method to improve the volume stability of SSA [7]. Steel slag is also rich in silicate minerals (dicalcium silicate,  $C_2S$ , and tricalcium silicate,  $C_3S$ ). These minerals undergo the carbonization reaction during the weathering period of SSA. The relatively higher temperature can promote the carbonization reaction [33] which means the volume expansion would be more obvious when SSA is sent to the hot water damage. In addition, the carbonation product layer wrapped on the surface of SSA is sensitive to the water freeze-thaw damage (temperature alternately changes) [35]. Meanwhile, the carbonation process also makes the SSFA agglomerate and consolidate. Its particle gradation and rich angular feature are destroyed. As a result, the material properties of SSFA are poor [7,32]. In addition, like other typical solid wastes, the material properties of steel slag fluctuate greatly [36].

Considering that there are some disadvantages when using SSA in asphalt concrete, developing a new reuse method for steel slag is urgent. In asphalt concrete, except for aggregate and asphalt, there is also a small proportion of filler. It participates in forming asphalt mastic with asphalt binder. The asphalt mastic helps to fill and glue the aggregate skeleton of asphalt concrete [37]. Hence, the filler is very important to the performance of asphalt concrete. Inspired by it, the feasibility of using steel slag powder (SSP) as a filler for asphalt concrete was investigated in this research. There are already some studies on the application of SSP in asphalt concrete [36,38,39]. Li et al. indicated that SSP is a high-alkalinity material; it improves the crack resistance of asphalt concrete based on the results of fracture energy [39]. Tao et al. suggested that for a combined filler composed of common limestone powder (LP) and SSP the suitable percentage of SSP is lower than 75% [38]. The research conducted by Chen et al. showed that compared to SSA, the properties of SSP are more homogeneous and stable. Asphalt concrete incorporating SSP shows satisfactory engineering performance [36]. Although some research has been performed on the use of SSP filler in asphalt concrete, these works mentioned above mainly focus on the steel

slag from the Wuhan iron and steel group, China (now called Baowu steel group, Wuhan, China). China has a vast territory; for the steel plants located in different regions, there are more or less differences in the steelmaking process and the types of raw materials used for steelmaking, which will finally influence the material properties of steel slag. Therefore, for the steel slag of each steel plant, especially the large plants such as the Baowu steel group, the Shougang group (Beijing, China), the Baogang group (Baotou, inner Mongolia, China), etc., it is necessary to conduct independent research on the feasibility of using SSPs from different steelmaking plants as fillers of asphalt concrete. In this research, steel slag from the Baogang group, China, was used. In addition, as mentioned earlier, steel slag is sensitive to the combined damage of temperature and moisture. While the previous studies mainly examined the changes in mechanical performance indexes after the combined damage, such as the retained Marshall stability (*RMS*) after hot water damage and tensile strength ratio (*TSR*) after freeze-thaw cycle damage [31,36], the effect of the combined damage on other performances of asphalt concrete such as high-temperature deformation resistance, low-temperature crack resistance, fatigue crack resistance, etc., is rarely evaluated.

Based on the above, the material properties of SSP prepared by grinding steel slag with a size of 2.36–4.75 mm from the Baogang group, China, and the main engineering performance of asphalt concrete incorporating this SSP under the combined damage of temperature and moisture were investigated in this research. The conducted work includes the following. (1) Preparing SSP by grinding steel slag (2.36–4.75 mm) in the laboratory first and then evaluating its material properties including the specific surface area, particle gradation, apparent density, chemical compositions, and thermal stability. Steel slag (2.36–4.75 mm) and common limestone powder (LP) filler were used as control groups. The grindability of steel slag and the advantages of using SSP as a filler in asphalt concrete were analyzed based on the results of material properties. (2) Using the Superpave method to design asphalt concrete incorporating SSP and LP. Then investigating the effect of the combined damage of temperature and moisture on the main engineering performance of asphalt concrete including volume stability (volume expansion test), mechanical performance (*RMS* and *TSR* tests), high-temperature deformation resistance (dynamic creep test), low-temperature crack resistance (indirect tensile test), and fatigue crack resistance (indirect tensile fatigue test). Two combined damage modes were used: hot water damage and freeze-thaw cycle damage. The feasibility of using SSP as a filler was further determined based on the results of the engineering performance of asphalt concrete. The research flow chart is shown in Figure 1.

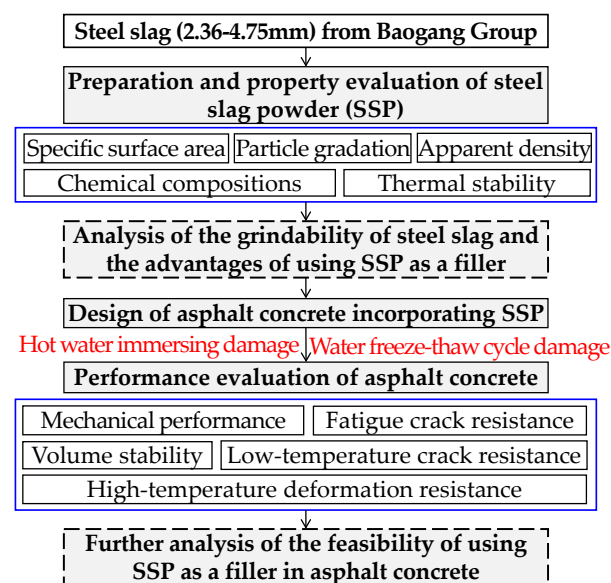


Figure 1. Research flow chart.

## 2. Materials and Methods

### 2.1. Raw Materials

The crushed basalt (9.5–19 mm and 4.75–9.5 mm) and limestone (0–4.75 mm) were used as a coarse aggregate and fine aggregate, respectively. They were from a crushed stone processing factory located in the Xilinhot, China. Steel slag was provided by the Baogang group located in inner Mongolia, China. In order to prepare steel slag powder (SSP) more easily in the laboratory, steel slag with a small particle size (2.36–4.75 mm) was sent to the ball mill for grinding. To compare the convenience of preparing SSP and common limestone powder (LP), limestone particles (2.36–4.75 mm) screened from the limestone fine aggregate (0–4.75 mm) were also adopted to prepare LP by a ball mill in the laboratory. In addition, an SBS-modified asphalt produced by inner Mongolia Yadong Asphalt Co., Ltd., Ordos, China, was also used.

Considering that all raw materials are produced in China and the terminal application scenario of designed asphalt concrete is also Chinese asphalt pavement, the basic technical properties of raw materials were tested according to the Chinese standard test methods [40,41]. The test results of basalt coarse aggregate, limestone fine aggregate, and SBS-modified asphalt are listed in Tables 1–3 which indicate that their basic technical properties meet the requirements of the Chinese technical specification [42]. The material properties of steel slag (2.36–4.75 mm), SSP, and LP will be discussed in detail in Section 3.1, so their basic technical properties are not shown here.

**Table 1.** Technical properties of basalt coarse aggregate.

Properties	Size Range (mm)	Results	Requirements
Apparent relative density	9.5–19	2.911	≥2.6
	4.75–9.5	2.903	
Water absorption (%)	9.5–19	0.4	≤2
	4.75–9.5	0.7	
Crushing value (%)	9.5–13.2	16.9	≤26
Elongated particle contents (%)	4.75–19	6.8	≤15
Los Angeles abrasion (%)	4.75–16	15.3	≤28

**Table 2.** Technical properties of limestone fine aggregate.

Properties	Results	Requirements
Apparent relative density	2.709	≥2.5
Soundness (%)	3.7	≤12
Fine aggregate angularity (%)	60	≥30
Sand equivalent (%)	66	≥60

**Table 3.** Technical properties of SBS-modified asphalt.

Properties	Results	Requirements
Ductility (5 °C, 5 cm/min; cm)	37.8	≥20
Softening point (°C)	78.5	≥60
Penetration (25 °C, 100 g, 5 s; 0.1 mm)	56	40–60
Viscosity (135 °C; Pa·s)	1.0	≤3
Elasticity resume (25 °C; %)	78	≥75
Solubility (%)	99.2	≥99

### 2.2. Experimental Methods

#### 2.2.1. Material Property Evaluation of SSP

Firstly, using a small-sized SM  $\Phi 500 \times 500$  mm ball mill with a rotation speed of 48 r/min to grind a total of 5 kg of steel slag and limestone particles (2.36–4.75 mm) for 20 min, 40 min, 60 min, and 80 min, and then the grindability of steel slag and limestone

particles was compared based on the test results of the specific surface area and particle gradation of SSP and LP. The specific surface area was determined by a fully automatic FBT-9 specific surface area tester, from the Zhongshuo, Hebei, China. The particle gradation was analyzed by a screening test.

The advantages of using SSP as a filler in asphalt concrete were preliminarily analyzed based on the test results of apparent density, chemical compositions, and thermal stability. The apparent density and chemical compositions of steel slag (2.36–4.75 mm), SSP, and LP were analyzed by the Chinese standard test method [40] and Zetium X-ray fluorescence (XRF) from the PANalytical, Almelo, Netherlands. The thermal stability of SSP during the mixing temperature range of asphalt concrete was evaluated by a discovery thermogravimetric analyzer (TGA) from TA Instruments, New Castle, DE, USA.

### 2.2.2. Design of Asphalt Concretes

The Superpave design method of asphalt concrete is one of the important achievements of the strategic highway research program (SHRP), which has been widely proven to be more in line with the actual construction situation of asphalt pavement. Therefore, in this research, the Superpave method was also used to design asphalt concrete incorporating SSP and LP. The designed air void of asphalt concrete was 4%. The volume dosage of basalt coarse aggregate (9.5–19 mm), basalt coarse aggregate (4.75–9.5 mm), limestone fine aggregate (0–4.75 mm), and filler (SSP and LP) was 23%, 29%, 44%, and 4%, respectively. The hybrid gradations of these two asphalt concretes are shown in Figure 2. The design results of the volumetric properties of asphalt concrete are listed in Table 4. It shows that the main volumetric property indexes of two asphalt concretes meet the design requirements.

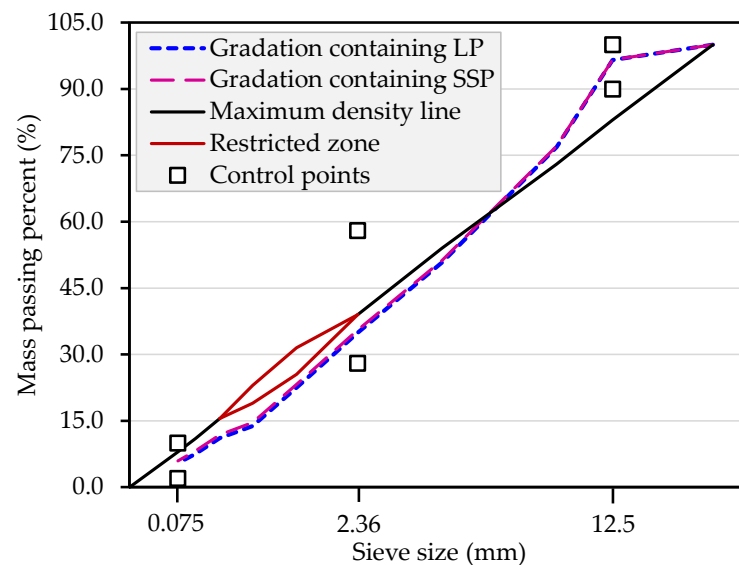


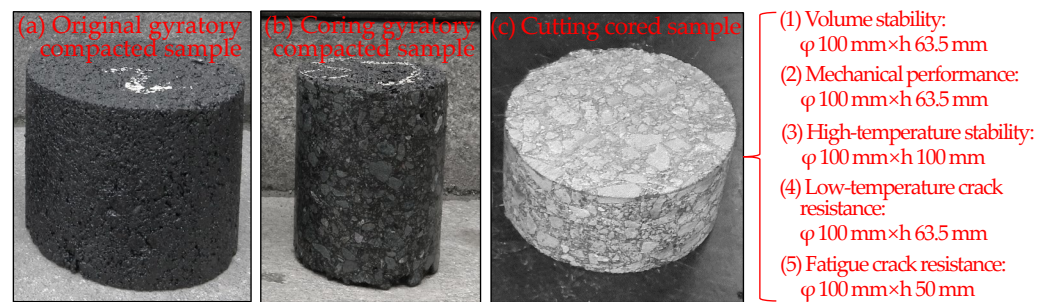
Figure 2. Hybrid gradations used in this research.

Table 4. Design results of asphalt concrete incorporating SSP and LP.

Volumetric Properties	Asphalt Concrete with SSP	Asphalt Concrete with LP	Design Requirements
Optimum asphalt content (OAC) (%)	4.8	4.8	—
Air voids (%)	4	4	4
Voids in the mineral aggregate (VMA) (%)	14.2	14.4	≥14
Voids filled with asphalt (VFA) (%)	71.8	72.2	65–75

### 2.2.3. Performance Evaluation of Asphalt Concretes under the Combined Damage of Temperature and Moisture

Preparation of samples for different performance evaluation. The Superpave design method is implemented based on the volumetric performance results of cylindrical specimens with a diameter of 100 mm and a height exceeding 100 mm, compacted in the Superpave gyratory compactor. Therefore, the samples used for evaluating performance of asphalt concrete were prepared by coring and cutting the Superpave gyratory compacted samples. Finally, samples with a diameter of 100 mm and a height of 63.5 mm were used in the evaluation of volume stability, mechanical performance, and low-temperature crack resistance. Samples with a diameter of 100 mm and a height of 100 mm and 50 mm were used in the evaluation of high-temperature deformation resistance and fatigue crack resistance, respectively. The preparation process and the sizes of used samples are shown in Figure 3.



**Figure 3.** Preparation process and sizes of used samples.

Selection of combined damage conditions of temperature and moisture. Two combined damage conditions of temperature and moisture were applied: hot water damage and freeze-thaw cycle damage. For hot water damage, the conditioned samples for each performance test were immersed in a hot water bath of 60 °C for 1 day, 2 days, and 3 days. For freeze-thaw cycle damage, the conditioned samples for each performance test were subjected to freeze-thaw damage for 1 cycle, 2 cycles, and 3 cycles. Single freeze-thaw cycle damage consists of freezing water-saturated samples in a freezer at −18 °C for 16 h and then thawing samples at a water bath of 60 °C for 24 h.

Volume stability evaluation. The volume stability of asphalt concrete was determined based on the volume expansion ratio. As shown in Equation (1), it was computed based on the changes in diameter and height of the sample after hot water damage or freeze-thaw cycle damage.

$$ve_r = \frac{d_2^2 h_2 - d_1^2 h_1}{d_1^2 h_1} \times 100\% \quad (1)$$

where  $ve_r$  is the volume expansion ratio, %;  $d_1$  and  $h_1$  are the original diameter and height of sample, respectively, mm; and  $d_2$  and  $h_2$  are the diameter and height of sample after hot water damage or freeze-thaw cycle damage, respectively, mm.

Mechanical performance evaluation. The Marshall stability of the sample before and after hot water damage was measured by an LWD-3C tester. The retained Marshall stability ( $RMS$ ) was computed by Equation (2). The indirect tensile strength ( $ITS$ ) of the sample before and after freeze-thaw cycle damage was computed by Equation (3) and the failure load of the sample was also measured by the LWD-3C tester. The tensile strength ratio ( $TSR$ ) was computed by Equation (4).

$$RMS = \frac{MS_2}{MS_1} \times 100\% \quad (2)$$

$$ITS = \frac{2000 \times P}{\pi \times D \times h} \quad (3)$$

$$TSR = \frac{ITS_2}{ITS_1} \times 100\% \quad (4)$$

where  $MS_1$  and  $MS_2$  are the Marshall stability of the sample before and after hot water damage, kN;  $P$  is the failure load of the sample, kN;  $D$  is the diameter of the sample, mm;  $h$  is the height of sample, mm; and  $ITS_1$  and  $ITS_2$  are the  $ITS$  of sample before and after freeze-thaw cycle damage, MPa.

**High-temperature deformation resistance.** The high-temperature stability of asphalt concrete was evaluated by a dynamic creep test. The samples for each asphalt concrete before and after hot water damage or freeze-thaw cycle damage were sent to a UTM-130 machine for a dynamic creep test. The test temperature was 60 °C. Samples were sent to the UTM-130 chamber for heat preservation for at least four hours in advance. The stress of 100 kPa with a haversine load pulse at 1 Hz (stop loading for 0.9 s after loading for 0.1 s) was applied. The general deformation process of the sample under the dynamic creep test is shown in Figure 4. The deformation process consists of three stages. In the first stage, the deformation speed of the sample decreases rapidly and it maintains at a stable value in the second stage, while the deformation speed rapidly increases when entering the third stage. As a result, the accumulated deformation sharply rises in this stage. It means that the deformation resistance ability of the sample rapidly decreases. Therefore, the number of cyclic loading corresponding to the starting point of the third stage, flow number ( $N_{instability}$ ), is frequently adopted to show the ultimate ability of asphalt concrete to resist high-temperature deformation [43,44]. The high-temperature stability of asphalt concrete was also determined based on the  $N_{instability}$  value in this research.

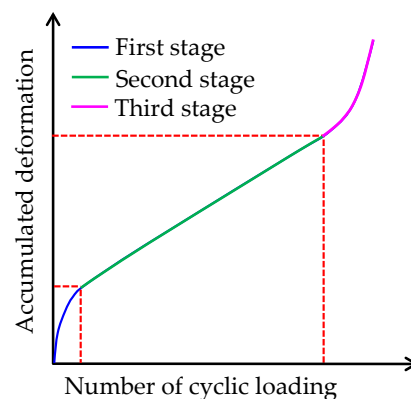


**Figure 4.** Deformation characteristics of the sample under the dynamic creep test.

**Low-temperature crack resistance.** The low-temperature crack resistance of asphalt concrete was analyzed based on the test results of the indirect tensile test. The samples for each asphalt concrete before and after hot water damage or freeze-thaw cycle damage were sent to the UTM-130 machine for an indirect tensile test by applying a constant deformation speed of 1 mm/min. The test temperature was −10 °C. The real-time load and deformation on the sample were automatically recorded by the computer. Then, the real-time stress and strain of the sample can be computed. Finally, the fracture energy index could be further determined according to Equation (5). The low-temperature crack resistance of asphalt concrete was quantized by the fracture energy index in this research.

$$fe = 10^{-3} \int_0^{\epsilon_f} \sigma(\epsilon) d\epsilon \quad (5)$$

where  $fe$  is the fracture energy, kJ/m<sup>3</sup>;  $\sigma(\epsilon)$  is the  $ITS$  of the sample when the strain is  $\epsilon$ , MPa; and  $\epsilon_f$  is the failure strain of sample,  $\mu\epsilon$ .

**Fatigue crack resistance.** The fatigue crack resistance of asphalt concrete was analyzed based on the test results of the indirect tensile fatigue test (ITFT). The ITFT of samples

for each asphalt concrete before and after hot water damage or freeze-thaw cycle damage was also conducted by the UTM-130 machine. The stress control mode with a total of four stress levels (0.35 MPa, 0.45 MPa, 0.55 MPa, and 0.65 MPa) was used and the loading frequency of the haversine load was 10 Hz. The test temperature was 20 °C. The test was terminated when a crack completely penetrated the sample and the number of cyclic loading at this point in time was regarded as the fatigue life of asphalt concrete. The fatigue crack resistance of asphalt concrete was determined by the value of fatigue life and its relationship with the stress level.

### 3. Results and Discussions

#### 3.1. Material Properties of Raw Materials

##### 3.1.1. Grindability of Steel Slag

The relationship between the specific surface area of SSP and LP and the grinding time during the grinding period of steel slag and limestone particles (2.36–4.75 mm) are shown in Figure 5. It can be seen that the specific surface area of SSP and LP both significantly increase with the extension of grinding time. It contributes to the size reduction in steel slag and limestone particles in the grinding process. In general, the specific surface area of SSP is always lower than that of LP after grinding for the same time. It suggests that the particles of LP are finer than SSP, namely, steel slag is more difficult to grind than limestone. Figure 5 also shows that the difference in specific surface area between SSP and LP gradually amplifies when the grinding time exceeds 40 min. The specific surface areas of SSP are 296 m<sup>2</sup>/kg after grinding for 60 min and 351 m<sup>2</sup>/kg after grinding for 80 min, respectively. They are 11.6% and 11.8% lower than that of LP, respectively. Results further indicate that the grindability of steel slag becomes worse as the grinding time prolongs. This is because steel slag contains some iron and because complex RO phases consist of multiple metal oxides. It is difficult to fully grind them. As the grinding time increases, the remaining ungrounded steel slag particles contain a higher proportion of iron and RO, making the grinding process more difficult.

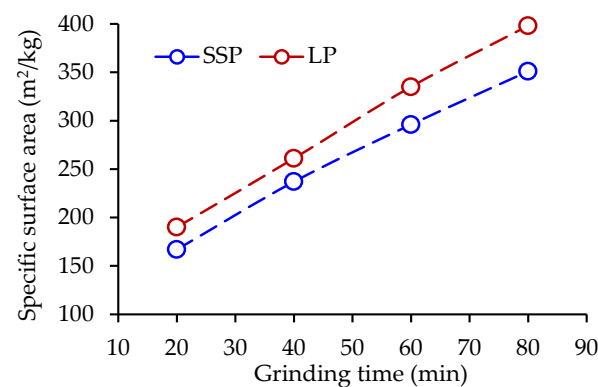


**Figure 5.** Changes in specific surface area of SSP and LP with grinding time.

According to the requirements of the Chinese technical specification [42], the maximum particle size of filler used in asphalt concrete should be no more than 0.6 mm. Therefore, particles larger than 0.6 mm in SSP and LP after grinding for 80 min were removed through screening. The particle gradations of SSP and LP used in subsequent studies are shown in Figure 6. It can be seen that the particle gradations of SSP and LP both meet the requirements of technical specification. Meanwhile, the difference between these two gradations is also very obvious. The passing percent of SSP corresponding to sieve sizes of 0.075 mm, 0.15 mm, and 0.3 mm are 83.5%, 91.4%, and 97.3%, respectively, which for LP are 88.3%, 95.3%, and 100%, respectively. The gradation results also support the conclusion that the grindability of steel slag is poorer than that of limestone.

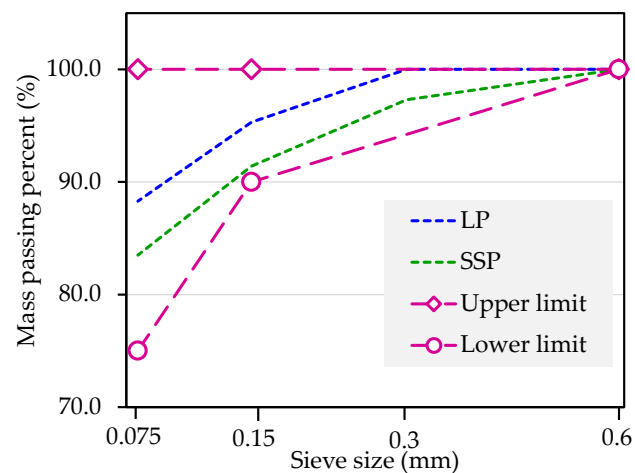


**Figure 6.** Particle gradations of SSP and LP.

### 3.1.2. Advantages of Using SSP in Asphalt Concrete

The average apparent densities of five randomly selected samples of SSA (steel slag aggregate with a particle size of 2.36–4.75 mm and raw materials for preparing SSP), SSP, and LP are presented in Figure 7. It shows that the densities of SSA and SSP are obviously bigger than that of LP. In detail, the densities of SSA and SSP are 3.345 g/cm<sup>3</sup> and 3.313 g/cm<sup>3</sup>, respectively, while the density of LP is only 2.701 g/cm<sup>3</sup>. This is also attributed to the contribution of high-density iron-related minerals (metal iron, iron oxide, and complex RO) in steel slag. Meanwhile, the density of SSP is about 0.96% lower than that of SSA. Although the difference is small, it also indicates, to some extent, that steel slag is difficult to grind. Some iron-related minerals which are difficult to grind remain in incompletely ground SSA after grinding for 80 min, which results in the density of SSP being relatively lower than that of SSA. Although the density of SSP is higher than that of common LP, the increase in transportation cost caused by the SSP filler would not be significant because the usage of filler in asphalt concrete is quite small (for example, the filler only accounts for 4% of the total mineral mixture by volume in this research). Another striking feature in Figure 7 is the size of the error bar. The sizes of the error bars corresponding to the test results of the apparent density of SSP and LP are much smaller than those of SSA. It indicates that multiple parallel test results of the apparent density of SSP and LP are more stable. It also proves that the properties of steel slag have been homogenized after grinding SSA into powder and that SSP possesses more uniform material properties. This characteristic is very beneficial for the stable utilization of SSP in asphalt concrete.

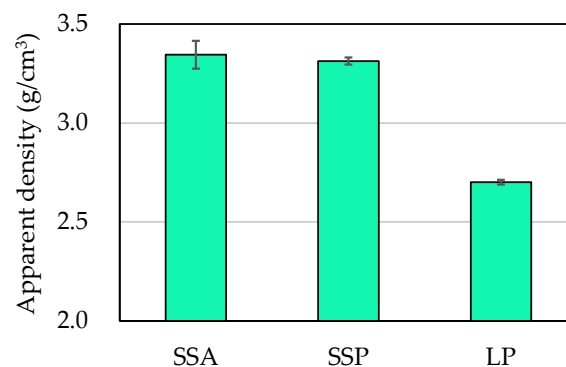


**Figure 7.** Apparent density results of SSA, SSP, and LP.

Although the component of steel slag is very complex, it is well known that steel slag mainly contains silicate minerals (tricalcium silicate, C<sub>3</sub>S, and dicalcium silicate, C<sub>2</sub>S) and

iron-related minerals (Fe, FeO, Fe<sub>2</sub>O<sub>3</sub>, complex RO solid solution composed of oxides of iron and other elements, etc.) [7,33]. In addition, it also contains some free lime (f-CaO) [7], free magnesium oxide (f-MgO) [35], and calcite (CaCO<sub>3</sub>) [33]. Therefore, the contents of Ca, Si, and Fe elements in steel slag would be quite large. The main chemical compositions of SSA and SSP (content greater than 5%), provided by XRF analysis in the form of elemental oxides, are presented in Figure 8. CaO, SiO<sub>2</sub>, Fe<sub>2</sub>O<sub>3</sub>, and MgO are the main chemical compositions of SSA and SSP. CaO and SiO<sub>2</sub> mainly belong to silicate minerals. Fe<sub>2</sub>O<sub>3</sub> and MgO mainly belong to iron-related minerals. Figure 8 also clearly presents that fact that the contents of CaO and SiO<sub>2</sub> in SSP are higher than that in SSA while the content of Fe<sub>2</sub>O<sub>3</sub> in SSP is obviously lower than that in SSA. Hence, the XRF results also support the conclusion that steel slag is difficult to grind and that some iron-related minerals remain in incompletely ground SSA after grinding for 80 min, which results in the content of Fe<sub>2</sub>O<sub>3</sub> in SSP being relatively lower than that in SSA.

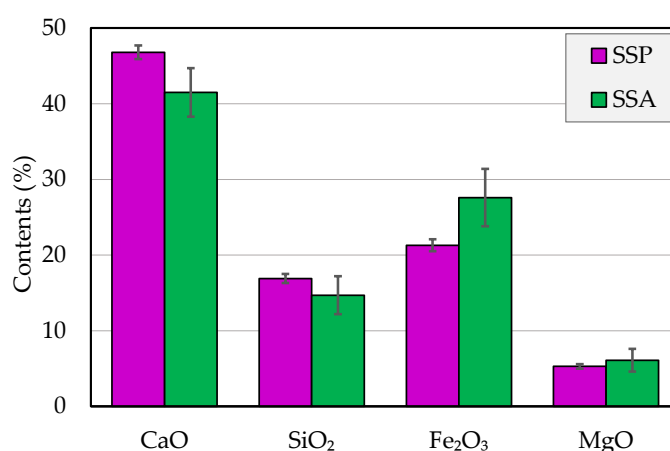


**Figure 8.** Main chemical compositions of SSA and SSP are given by XRF analysis.

The XRF results can demonstrate the advantages of SSP as a filler for asphalt concrete from two aspects. One is the excellent uniformity of material properties. Figure 8 also shows that the sizes of the error bars corresponding to the contents of the main chemical compositions of SSP are much smaller than that of SSA (each group also underwent five repeated tests). Chen et al. analyzed the chemical compositions of SSA and SSP from the China Baowu steel group and they also proved that the contents of the main chemical composition of SSP are more stable [36]. Therefore, the XRF results further confirm that grinding SSA into SSP also improves the uniformity of material properties of steel slag, which helps to realize the stable utilization of SSP in asphalt concrete. The other aspect is the high alkalinity of SSP. Steel slag is usually divided into three categories according to its alkalinity: low alkalinity steel slag (alkalinity below 1.8), intermediate alkalinity steel slag (alkalinity between 1.8 and 2.5), and high alkalinity steel slag (alkalinity beyond 2.5) [45]. The alkalinity can be computed based on the analysis results of chemical compositions as  $w(\text{CaO})/[w(\text{SiO}_2) + w(\text{P}_2\text{O}_5)]$ . The computed alkalinities of SSA and SSP are 2.61 and 2.64, respectively (the contents of P<sub>2</sub>O<sub>5</sub> in SSA and SSP are 1.2% and 0.8%, respectively). So, SSA and SSP are high-alkalinity steel slag. Previous research also confirmed that the steel slag from Baowu steel group is also high alkalinity steel slag [36]. It indicates that the steel slag produced by large steel plants in China is mainly highly alkaline slag. In order to improve the bonding strength and engineering performance of asphalt concrete, some alkaline fillers are frequently adopted to modify asphalt mastic, such as hydrated lime [46]. Hence, the high alkalinity feature of SSP gives it an advantage for use in asphalt concrete.

The mixing temperature of asphalt concrete will be less than 200 °C even for the modified asphalt concrete. To determine whether SSP can maintain stability at the mixing temperature of asphalt concrete, the thermal stability of SSP during the mixing temperature range of asphalt concrete was further analyzed based on the measure results of TGA, as

shown in Figure 9. It can be seen that the mass loss of SSP is only about 0.5% when the temperature rises from room temperature to 200 °C. The mass change in SSP is quite small. The DSC curve further shows that there is an endothermic peak and the temperature to the top of the peak is about 79.5 °C. This corresponds to the evaporation of free water in SSP. Therefore, the compositions of SSP remain stable during the mixing temperature of asphalt concrete. SSP shows good thermal stability.

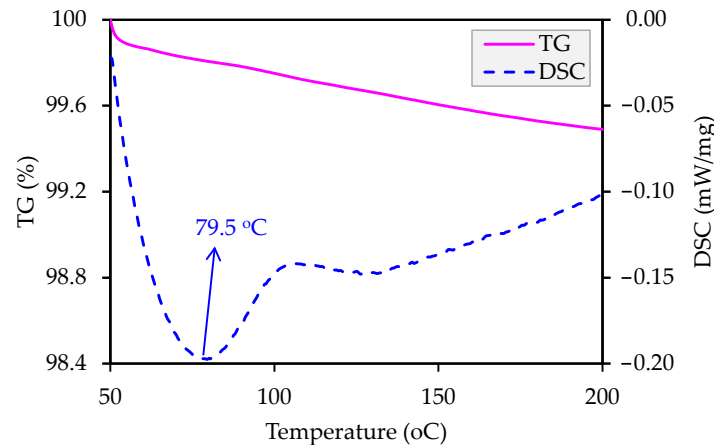


**Figure 9.** Thermal stability analysis result of SSP.

### 3.2. Effect of the Combined Damage of Temperature and Moisture on the Engineering Performance of Asphalt Concrete Incorporating SSP

In this section, five aspects of engineering performance of asphalt concrete were analyzed: volume stability, mechanical performance, high-temperature deformation resistance, low-temperature crack resistance, and fatigue crack resistance. All presented results are average value computed based on five parallel tests. For convenience, asphalt concrete incorporating SSP and asphalt concrete incorporating LP were referred to as AC-SSP and AC-LP in the following text, respectively.

#### 3.2.1. Volume Stability

Volume stability test results of asphalt concrete under the hot water damage mode and freeze-thaw cycle damage mode are shown in Figures 10 and 11, respectively. Figure 10 shows that the volume expansion ratio of AC-SSP and AC-LP both gradually increase as the hot water damage time prolongs, although their growth patterns are different. In general, the expansion behavior of these two asphalt concretes under hot water damage are very weak. The volume expansion ratio of AC-SSP and AC-LP is only 0.68% and 0.63%, respectively, even after hot water damage for 3 days. There is no significant difference in volume expansion ratio between these two asphalt concretes. It indicates that the  $f$ -CaO in did not cause obvious volume expansion, which is attributed to the excellent uniformity of material properties of SSP, low usage of SSP in asphalt concrete, and effective wrapping behavior of asphalt to SSP. It is also consistent with the previous finding [36]. The Chinese technical specification sets a requirement on the volume expansion ratio of asphalt concrete under hot water damage: it should be no more than 1.5% after the asphalt concrete sample is subjected to hot water damage for 3 days. AC-SSP can easily meet this requirement. Therefore, the introduction of SSP filler has not worsened the volume stability of asphalt concrete under hot water damage.

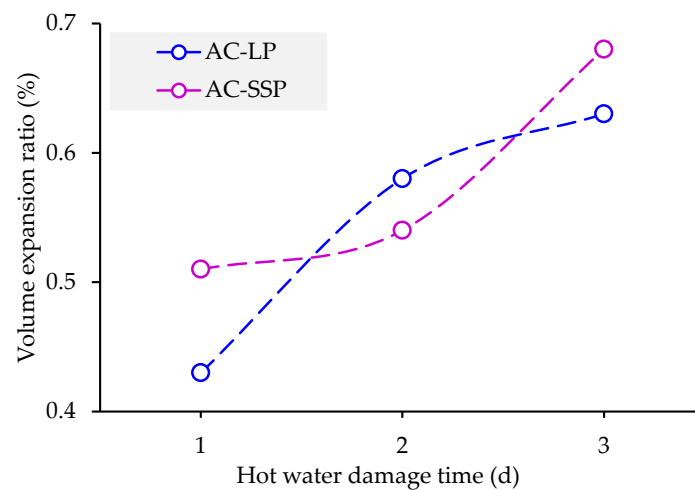


**Figure 10.** Volume expansion ratio results of hot water-damaged asphalt concrete.

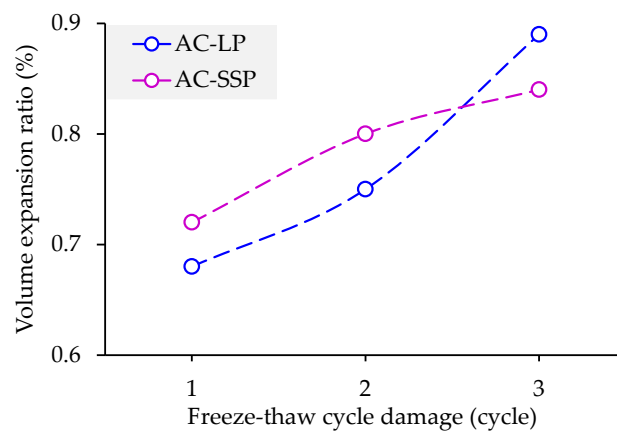


**Figure 11.** Volume expansion ratio results of freeze-thaw cycle-damaged asphalt concrete.

Figure 11 also shows that there is no significant difference in the volume expansion ratio between these two asphalt concretes under the freeze-thaw cycle damage mode. It indicates that the  $f$ -CaO in SSP still keeps stable under this damage mode and that AC-SSP also presents satisfactory volume stability. Therefore, the volume expansion phenomenon of AC-SSP and AC-LP is attributed to the change in water during the cyclic freeze-thaw process. Figure 11 further presents that for either AC-SSP or AC-LP, compared to the hot water damage mode, the volume expansion phenomenon is slightly more obvious under the freeze-thaw cycle damage mode. The volume expansion ratio of both AC-SSP and AC-LP is around 0.7% even if just one freeze-thaw cycle is applied. It suggests that the frost-heaving force of water inside the samples during the freezing period is more destructive.

### 3.2.2. Mechanical Performance

According to the Chinese technical specification [42], two mechanical performance indexes of asphalt concrete under the combined damage of temperature and moisture are required to be measured: Marshall stability after hot water damage and *ITS* after freeze-thaw cycle damage. The mechanical performance evaluation in this research was also conducted according to it.

The Marshall stability and *RMS* results of asphalt concrete after different times of hot water damage are listed in Figures 12 and 13, respectively. It can be seen that the original Marshall stability of AC-SSP is larger than that of AC-LP and that the former is about 13.2% bigger than the latter. So, the introduction of SSP filler improves the Marshall stability of asphalt concrete. The Marshall stability of AC-SSP and AC-LP both decreases to varying degrees with the increase in hot water damage time. It confirms that the Marshall stability

of asphalt concrete is sensitive to hot water damage. Figure 13 shows that AC-LP has a more significant fall in Marshall stability with the increase in hot water damage time; the loss of Marshall stability reaches 11.3% when the hot damage time increases to 3 days. For AC-SSP, the loss is 9.7%. So, compared to AC-LP, AC-SSP shows better mechanical performance in terms of Marshall stability even after serious combined damage of high temperature and moisture. This may be attributed to the strong alkalinity feature of SSP. The strong alkalinity of SSA and SSP has been widely proven to enhance the bonding strength and moisture-induced damage resistance of asphalt concrete [33,36,47]. This is because asphalt is a weakly acidic material and it shows better bonding performance with alkaline aggregates such as SSA. For SSP, SSP particles form alkaline sites on the surface of aggregates also help to enhance the bonding performance between asphalt and aggregates.

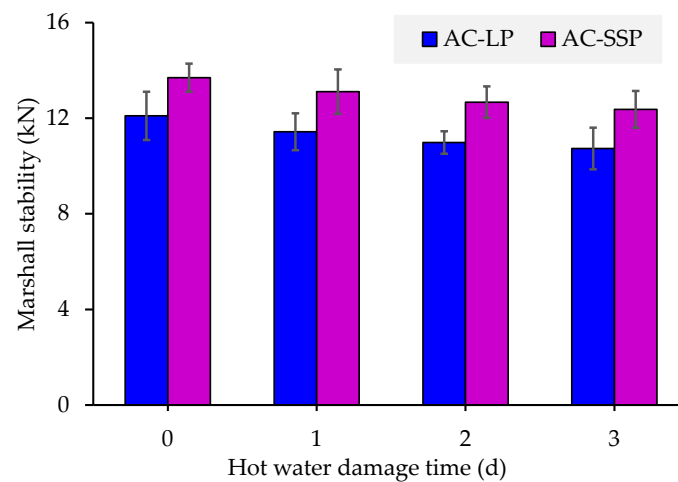


**Figure 12.** Marshall stability results of hot water-damaged asphalt concrete.

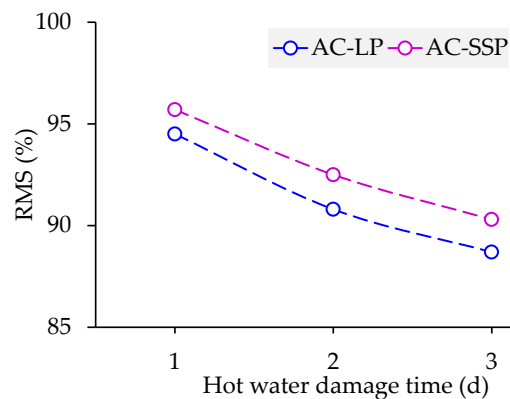


**Figure 13.** RMS results of hot water-damaged asphalt concrete.

The *ITS* and *TSR* results of asphalt concrete after different numbers of freeze-thaw cycle damage are presented in Figures 14 and 15, respectively. Figure 14 also shows that the original *ITS* of AC-SSP is larger and it is about 11.4% bigger than that of AC-LP. It confirms that SSP filler also improves the *ITS* of asphalt concrete. Similar to the changing trend of Marshall stability to hot water damage time, the *ITS* of AC-SSP and AC-LP both decrease to varying degrees with the increase in the number of freeze-thaw cycles. According to Figure 15, the *TSR* of AC-SSP and AC-LP after three cycles of freeze-thaw cycle damage is 84.9% and 82.6%, respectively. It means that the loss of *ITS* of AC-SSP and AC-LP reaches 15.1% and 17.4%, respectively. It confirms that the *ITS* of asphalt concrete is quite sensitive to freeze-thaw cycle damage and AC-SSP performs better in maintaining the *ITS* of asphalt concrete under freeze-thaw cycle damage. Therefore, compared to AC-LP, AC-SSP also

shows better mechanical performance in terms of *ITS* even facing a serious freeze-thaw cycle damage condition.

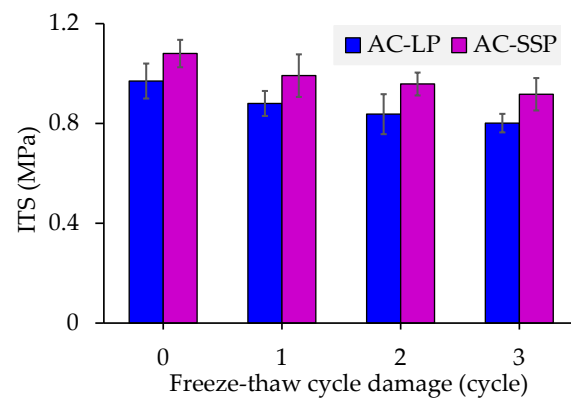


**Figure 14.** *ITS* results of freeze-thaw cycle-damaged asphalt concrete.

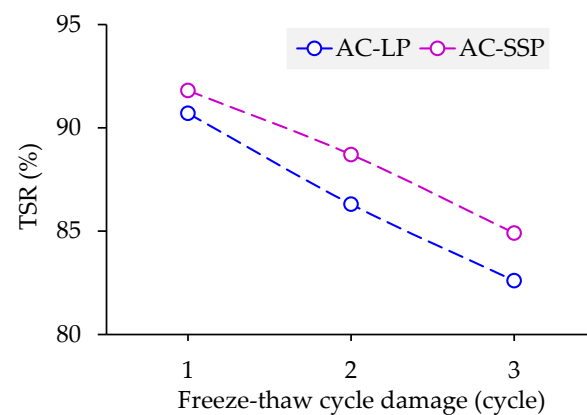


**Figure 15.** *TSR* results of freeze-thaw cycle-damaged asphalt concrete.

### 3.2.3. High-Temperature Deformation Resistance

The  $N_{\text{instability}}$  value was determined based on the dynamic creep test result. Figures 16 and 17 present the  $N_{\text{instability}}$  of hot water-damaged asphalt concrete and freeze-thaw cycle-damaged asphalt concrete, respectively. The embedded skeleton formed by aggregates is believed to be the main factor determining the high-temperature stability of asphalt concrete. Figures 16 and 17 show that the original  $N_{\text{instability}}$  of AC-SSP is a little higher than that of AC-LP. It suggests that the filler also affects the high-temperature deformation resistance of asphalt concrete. After hot water damage or freeze-thaw cycle damage is applied, the  $N_{\text{instability}}$  value of both AC-SSP and AC-LP gradually decreases as the hot water damage time or the number of freeze-thaw cycles increases. It proves that the combined damage of temperature and moisture worsened the high-temperature deformation resistance of asphalt concrete.

In addition, there are some differences in the variation characteristics of the  $N_{\text{instability}}$  of these two asphalt concretes under hot water damage and freeze-thaw cycle damage conditions. To Figure 16, the  $N_{\text{instability}}$  of AC-SSP is always more or less larger than that of AC-LP after suffering the same time of hot water damage which means that SSP plays a positive role in maintaining the high-temperature stability of asphalt concrete under hot water damage. The situation is a little different when referring to freeze-thaw cycle damage. Figure 17 displays that the  $N_{\text{instability}}$  of AC-SSP is not always bigger than that of AC-LP after suffering the same number of freeze-thaw cycle damage. The damage of the frost heaving force of water to the aggregate embedded skeleton during cyclic freeze-thaw process weakens the stability of embedded skeleton. However, the deterioration degree of the stability of the embedded skeleton is not entirely the same, even facing the same

number of freeze-thaw cycle damage, which is related to the initial status of the embedded skeleton of the used sample. So, the  $N_{\text{instability}}$  of AC-SSP is not always bigger than that of AC-LP. Although the effect of freeze-thaw cycle damage on the high-temperature stability of asphalt concrete is more obvious, the difference in  $N_{\text{instability}}$  between AC-SSP and AC-LP is small. Compared to AC-LP, the  $N_{\text{instability}}$  of AC-SSP is 1.7% lower (1 cycle), 1.1% lower (2 cycles), and 4.0% higher (3 cycles). It suggests that freeze-thaw-damaged AC-SSP and AC-LP still have comparable high-temperature performance; AC-SSP even does slightly better when facing serious freeze-thaw damage conditions.

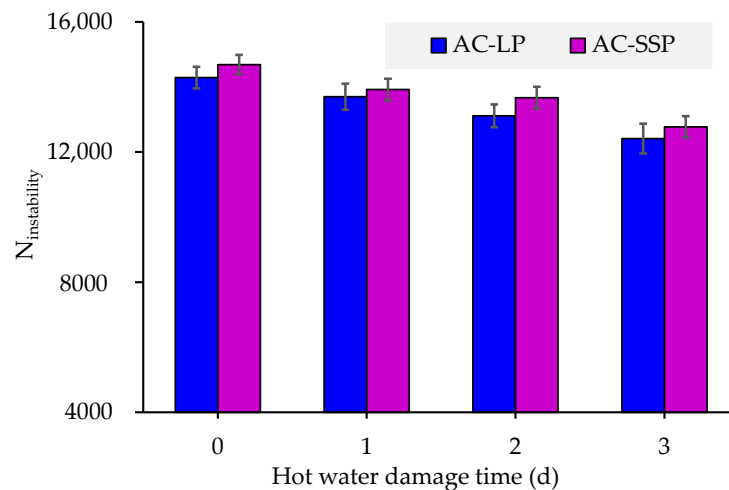


**Figure 16.**  $N_{\text{instability}}$  value of hot water-damaged asphalt concrete.

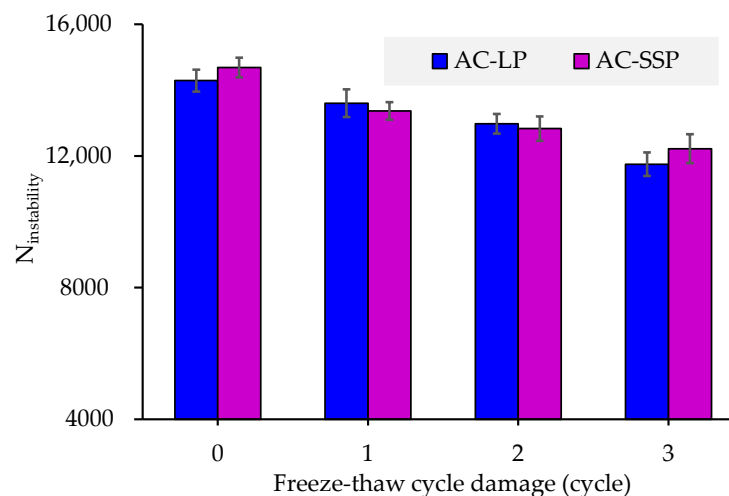


**Figure 17.**  $N_{\text{instability}}$  value of freeze-thaw cycle-damaged asphalt concrete.

### 3.2.4. Low-Temperature Crack Resistance

The fracture energy of hot water-damaged asphalt concrete and freeze-thaw cycle-damaged asphalt concrete is shown in Figures 18 and 19, respectively. These two figures display that the original fracture energy of AC-SSP is 8.7% higher than that of AC-LP. So, the introduction of SSP also improves the low-temperature crack resistance of asphalt concrete. However, whether under hot water damage or freeze-thaw cycle damage, the fracture energy of AC-SSP and AC-LP both shows a decreasing trend as the hot water damage time or the number of freeze-thaw cycles increases. It indicates that the combined damage of temperature and moisture also worsens the low-temperature crack resistance of asphalt concrete. In detail, although the decrease in fracture energy of AC-SSP and AC-LP after hot water damage for 3 days is relatively close (about 14%), compared to AC-LP, AC-SSP always shows larger fracture energy after suffering the same time of hot water

damage (see Figure 18). Therefore, SSP also performs a positive role in maintaining the low-temperature crack resistance of asphalt concrete even when facing a serious damage condition consisting of a high temperature and moisture. The advantage of SSP is not prominent when facing freeze-thaw cycle damage. Figure 19 shows that the difference in fracture energy between AC-SSP and AC-LP becomes small when the number of freeze-thaw cycle damage exceeds one cycle. It suggests that some other factors in the freeze-thaw period have affected the low-temperature crack resistance of asphalt concrete more significantly. For example, the changes in the stability of aggregate embedded skeleton and the bonding performance between aggregate and asphalt, caused by the frost-heaving force of water, will lead to changes in *ITS* and strain in asphalt concrete under indirect tensile test, which affect the fracture energy of asphalt concrete sharply. Compared to AC-LP, AC-SSP also presents comparable or better low-temperature crack resistance after the combined damage of temperature and moisture.

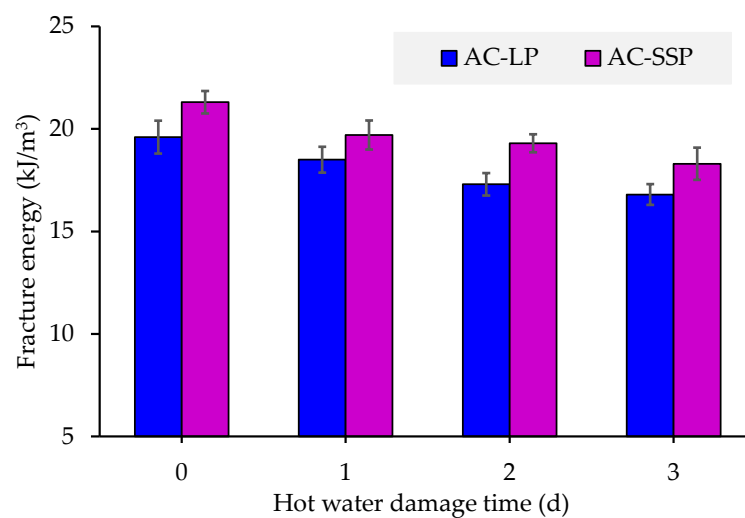


**Figure 18.** Fracture energy of hot water-damaged asphalt concrete.

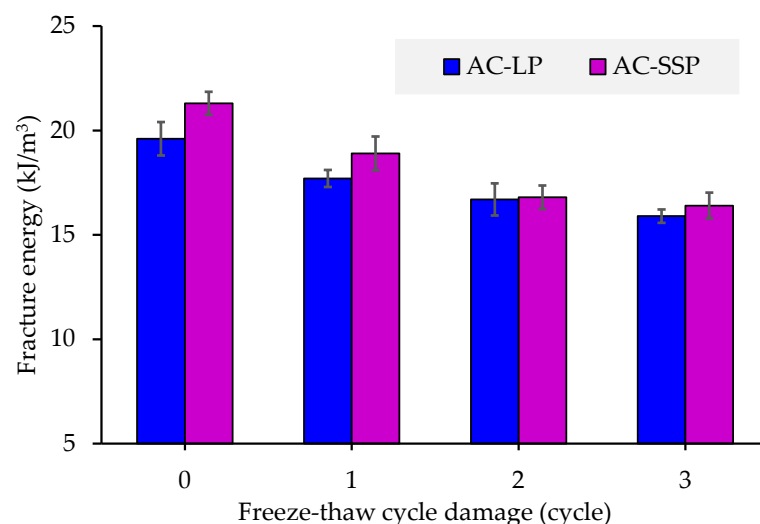


**Figure 19.** Fracture energy of freeze-thaw cycle-damaged asphalt concrete.

### 3.2.5. Fatigue Crack Resistance

The fatigue life of asphalt concrete at 0.35 MPa was adopted to analyze the effect of the combined damage of temperature and moisture on the fatigue life of asphalt concrete. As shown in Figures 20 and 21, after hot water damage and freeze-thaw cycle damage, the fatigue life of these two asphalt concretes both decreases and the loss of fatigue life

gradually rises with the increase in hot water damage time and freeze-thaw cycles. In detail, after hot water damage for 3 days, the fatigue life of AC-SSP and AC-LP is lost by 8.1% and 7.5%, respectively. After freeze-thaw cycle damage for three cycles, it was lost by 8.8% and 8.6%, respectively. This suggests that the combined damage of temperature and moisture also lowers the fatigue crack resistance of asphalt concrete.

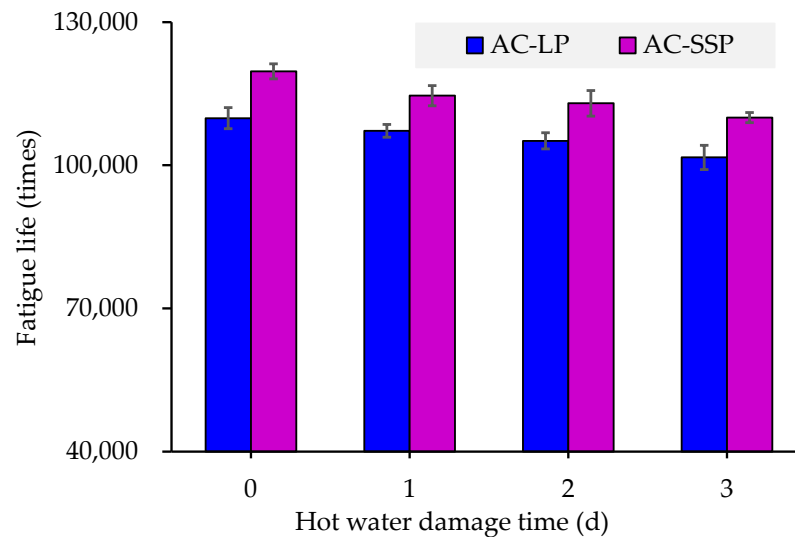


**Figure 20.** ITFT results of hot water-damaged asphalt concrete.

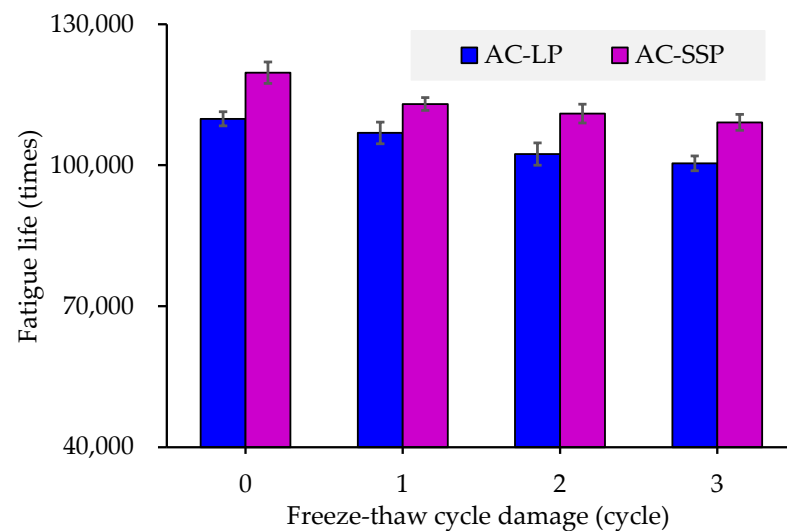


**Figure 21.** ITFT results of freeze-thaw cycle-damaged asphalt concrete.

Figures 20 and 21 also display that SSP plays a more positive role in improving the fatigue life of asphalt concrete. The original fatigue life of AC-SSP is about 8.9% larger than that of SSP-LP. Although the loss of fatigue life of AC-SSP after hot water damage for 3 days or freeze-thaw cycle damage for three cycles is a little larger than that of AC-LP, compared to AC-LP, the advantage of AC-SSP in terms of fatigue life is maintained during the combined damage of temperature and moisture. Even after hot water damage for 3 days, the fatigue life of AC-SSP is still 8.2% bigger than that of AC-LP, which is 8.7% after freeze-thaw cycle damage for three cycles. Therefore, AC-SSP also presents better fatigue crack resistance after the combined damage of temperature and moisture.

The fatigue life of asphalt concrete after hot water damage for 3 days and freeze-thaw cycle damage for three cycles at 0.35 MPa, 0.45 MPa, 0.55 MPa, and 0.65 MPa was further adopted to analyze the relationship between fatigue life and stress level. The power function, as shown in Equation (6), is very effective in modeling the relationship

between the fatigue life of asphalt concrete and the stress level. It is usually represented as a double logarithmic form as shown in Equation (7). The  $\log(f_{life})$  and  $\log(\sigma)$  have a linear relationship. The parameter  $\beta$  reflects the sensitivity of  $\log(f_{life})$  to  $\log(\sigma)$ .

$$f_{life} = \alpha\sigma^{-\beta} \quad (6)$$

$$\log f_{life} = -\beta \log \sigma + \log \alpha \quad (7)$$

where  $f_{life}$  is the fatigue life of asphalt concrete, times;  $\sigma$  is applied stress, MPa; and  $\alpha$  and  $\beta$  are constants related to the characteristics of asphalt concrete.

The fitting results of fatigue life to stress level (power function) of AC-SSP and AC-LP after suffering different conditions of damage are listed in Table 5. The high  $R^2$  value proves that using the power model to fit the relationship between the fatigue life of asphalt concrete and stress level is effective. Whether it is AC-SSP or AC-LP,  $\beta$  both increases after the combined damage of temperature and moisture; the increase is more significant after freeze-thaw cycle damage. It means the fatigue durability of asphalt concrete gets worse after the combined damage of temperature and moisture. The destructive ability of freeze-thaw cycles is stronger. Even so, when no any damage is applied or facing the same damage conditions, the  $\beta$  of AC-SSP is always lower than that of AC-LP. It indicates that the introduction of SSP improved the fatigue durability of original asphalt concrete, hot water-damaged asphalt concrete, and freeze-thaw cycle-damaged asphalt concrete.

**Table 5.** Fitting results of the fatigue life of asphalt concrete after different damage.

Damage Condition	Concrete Type	Fitting Result	$\beta$	$R^2$
Without damage	AC-LP	$f_{life} = 1442.3\sigma^{-4.147}$	4.147	0.99
	AC-SSP	$f_{life} = 1840.2\sigma^{-4.016}$	4.016	0.98
Hot water damage (3 days)	AC-LP	$f_{life} = 1138.6\sigma^{-4.316}$	4.316	0.97
	AC-SSP	$f_{life} = 1473.0\sigma^{-4.166}$	4.166	0.98
Freeze-thaw cycle damage (3 cycles)	AC-LP	$f_{life} = 857.9\sigma^{-4.597}$	4.597	0.99
	AC-SSP	$f_{life} = 1442.3\sigma^{-4.320}$	4.320	0.98

#### 4. Conclusions

In this work, the steel slag with a size of 2.36–4.75 mm from the Baogang group located in inner Mongolia, China, was first ground into SSP; the material properties of SSP and performance characteristics of asphalt concrete incorporating SSP filler after the combined damage of temperature and moisture were evaluated. The following conclusions can be drawn:

1. Steel slag (2.36–4.75 mm) is more difficult to grind compared to the limestone particles with the same size range. It is related to the rich contents of iron-related minerals. Improving the grindability of steel slag is an important direction that needs to be expanded in the future;
2. Grinding steel slag into SSP has improved the uniformity of its material properties. Good uniformity of material properties, high alkalinity, and excellent thermal stability of SSP give it some advantages for use in asphalt concrete;
3. The introduction of SSP in asphalt concrete improves the mechanical performance, high-temperature stability, low-temperature crack resistance, fatigue crack resistance, and fatigue durability of original asphalt concrete;
4. Compared to asphalt concrete with common limestone filler, asphalt concrete incorporating SSP filler possesses comparable or better engineering performance even after suffering the serious combined damage of temperature and moisture.

**Author Contributions:** Conceptualization, S.L.; Methodology, S.L. and Z.Z.; Investigation, S.L. and Z.Z.; Data curation, S.L.; Supervision, R.W.; Validation, R.W.; writing—original draft preparation, S.L.; writing—review and editing, S.L., Z.Z. and R.W.; funding acquisition, R.W. All authors have read and agreed to the published version of the manuscript.

**Funding:** This work was financially supported by the Science and Technology Project from the Transportation Department of Inner Mongolia (No. NJ-2022-21).

**Institutional Review Board Statement:** Not applicable.

**Informed Consent Statement:** Not applicable.

**Data Availability Statement:** Not applicable.

**Acknowledgments:** Thanks to the Transportation Department of Inner Mongolia for providing financial support.

**Conflicts of Interest:** The authors declare no conflict of interest.

## References

- Li, D.; Leng, Z.; Zou, F.; Yu, H. Effects of rubber absorption on the aging resistance of hot and warm asphalt rubber binders prepared with waste tire rubber. *J. Clean. Prod.* **2021**, *303*, 127082. [[CrossRef](#)]
- Yu, H.; Zhu, Z.; Leng, Z.; Wu, C.; Zhang, Z.; Wang, D.; Oeser, M. Effect of mixing sequence on asphalt mixtures containing waste tire rubber and warm mix surfactants. *J. Clean. Prod.* **2020**, *246*, 119008. [[CrossRef](#)]
- Kumar, H.; Varma, S. A review on utilization of steel slag in hot mix asphalt. *Int. J. Pavement Res. Technol.* **2021**, *14*, 232–242. [[CrossRef](#)]
- Fares, A.I.; Sohel, K.; Al-Jabri, K.; Al-Mamun, A. Characteristics of ferrochrome slag aggregate and its uses as a green material in concrete—A review. *Constr. Build. Mater.* **2021**, *294*, 123552. [[CrossRef](#)]
- Qasrawi, H. The use of steel slag aggregate to enhance the mechanical properties of recycled aggregate concrete and retain the environment. *Constr. Build. Mater.* **2014**, *54*, 298–304. [[CrossRef](#)]
- Wu, R.; Xiao, Y.; Zhang, P.; Lin, J.; Cheng, G.; Chen, Z.; Yu, R. Asphalt VOCs reduction of zeolite synthesized from solid wastes of red mud and steel slag. *J. Clean. Prod.* **2022**, *345*, 131078. [[CrossRef](#)]
- Chen, Z.; Jiao, Y.; Wu, S.; Tu, F. Moisture-induced damage resistance of asphalt mixture entirely composed of gneiss and steel slag. *Constr. Build. Mater.* **2018**, *177*, 332–341. [[CrossRef](#)]
- Wu, S.; Zhong, J.; Zhu, J.; Wang, D. Influence of demolition waste used as recycled aggregate on performance of asphalt mixture. *Road Mater. Pavement Des.* **2013**, *14*, 679–688. [[CrossRef](#)]
- Etxeberria, M.; Vázquez, E.; Mari, A.; Barra, M. Influence of amount of recycled coarse aggregates and production process on properties of recycled aggregate concrete. *Cem. Concr. Res.* **2007**, *37*, 735–742. [[CrossRef](#)]
- Taha, R.; Al-Harthy, A.; Al-Shamsi, K.; Al-Zubeidi, M. Cement stabilization of reclaimed asphalt pavement aggregate for road bases and subbases. *J. Mater. Civ. Eng.* **2002**, *14*, 239–245. [[CrossRef](#)]
- Magar, S.; Xiao, F.; Singh, D.; Showkat, B. Applications of reclaimed asphalt pavement in India—A review. *J. Clean. Prod.* **2022**, *335*, 130221. [[CrossRef](#)]
- Li, R.; Leng, Z.; Yang, J.; Lu, G.; Huang, M.; Lan, J.; Zhang, H.; Bai, Y.; Dong, Z. Innovative application of waste polyethylene terephthalate (PET) derived additive as an antistripping agent for asphalt mixture: Experimental investigation and molecular dynamics simulation. *Fuel* **2021**, *300*, 121015. [[CrossRef](#)]
- Xu, X.; Leng, Z.; Lan, J.; Wang, W.; Yu, J.; Bai, Y.; Sreeram, A.; Hu, J. Sustainable practice in pavement engineering through value-added collective recycling of waste plastic and waste tyre rubber. *Engineering* **2021**, *7*, 857–867. [[CrossRef](#)]
- Abdullah, B.A.O.; Jakarni, F.; Al-Shakhrit, A.; Masri, K.A. The usage of recycled glass in hot mix asphalt: A review. *Construction* **2021**, *1*, 29–34. [[CrossRef](#)]
- Su, N.; Chen, J. Engineering properties of asphalt concrete made with recycled glass. *Resour. Conserv. Recycl.* **2002**, *35*, 259–274. [[CrossRef](#)]
- Shi, C. Steel slag—Its production, processing, characteristics, and cementitious properties. *J. Mater. Civ. Eng.* **2004**, *16*, 230–236. [[CrossRef](#)]
- Kang, H.-J.; An, K.-G.; Kim, D.-S. Utilization of steel slag as an adsorbent of ionic lead in wastewater. *J. Environ. Sci. Health Part A* **2004**, *39*, 3015–3028. [[CrossRef](#)]
- González-Tolivia, E.; Collado, S.; Oulego, P.; Díaz, M. BOF slag as a new alkalizing agent for the stabilization of sewage sludge. *Waste Manag.* **2022**, *153*, 335–346. [[CrossRef](#)]
- Papastergiadis, E.; Sklari, S.; Zouboulis, A.; Chasiotis, A.; Samaras, P. The use of steelmaking slag for sewage sludge stabilization. *Desalination Water Treat.* **2015**, *55*, 1697–1702. [[CrossRef](#)]
- Reddy, K.R.; Gopakumar, A.; Chetri, J.K. Critical review of applications of iron and steel slags for carbon sequestration and environmental remediation. *Rev. Environ. Sci. Bio/Technol.* **2019**, *18*, 127–152. [[CrossRef](#)]

21. Mayes, W.M.; Riley, A.L.; Gomes, H.I.; Brabham, P.; Hamlyn, J.; Pullin, H.; Renforth, P. Atmospheric CO<sub>2</sub> sequestration in iron and steel slag: Consett, County Durham, United Kingdom. *Environ. Sci. Technol.* **2018**, *52*, 7892–7900. [[CrossRef](#)] [[PubMed](#)]
22. Islam, Z.; Tran, Q.T.; Koizumi, S.; Kato, F.; Ito, K.; Araki, K.S.; Kubo, M. Effect of steel slag on soil fertility and plant growth. *J. Agric. Chem. Environ.* **2022**, *11*, 209–221. [[CrossRef](#)]
23. Tsakiridis, P.E.; Papadimitriou, G.D.; Tsvivilis, S.; Koroneos, C. Utilization of steel slag for Portland cement clinker production. *J. Hazard. Mater.* **2008**, *152*, 805–811. [[CrossRef](#)] [[PubMed](#)]
24. Gencel, O.; Karadag, O.; Oren, O.H.; Bilir, T. Steel slag and its applications in cement and concrete technology: A review. *Constr. Build. Mater.* **2021**, *283*, 122783. [[CrossRef](#)]
25. Ferreira, V.J.; Vilaplana, A.S.-D.-G.; García-Armingol, T.; Aranda-Usón, A.; Lausín-González, C.; López-Sabirón, A.M.; Ferreira, G. Evaluation of the steel slag incorporation as coarse aggregate for road construction: Technical requirements and environmental impact assessment. *J. Clean. Prod.* **2016**, *130*, 175–186. [[CrossRef](#)]
26. Díaz-Piloneta, M.; Terrados-Cristos, M.; Álvarez-Cabal, J.V.; Vergara-González, E. Comprehensive analysis of steel slag as aggregate for road construction: Experimental testing and environmental impact assessment. *Materials* **2021**, *14*, 3587. [[CrossRef](#)]
27. Wu, S.; Xue, Y.; Ye, Q.; Chen, Y. Utilization of steel slag as aggregates for stone mastic asphalt (SMA) mixtures. *Build. Environ.* **2007**, *42*, 2580–2585. [[CrossRef](#)]
28. Pasetto, M.; Baliello, A.; Giacomello, G.; Pasquini, E. The Use of Steel Slags in Asphalt Pavements: A State-of-the-Art Review. *Sustainability* **2023**, *15*, 8817. [[CrossRef](#)]
29. Kehagia, F. Skid resistance performance of asphalt wearing courses with electric arc furnace slag aggregates. *Waste Manag. Res.* **2009**, *27*, 288–294. [[CrossRef](#)]
30. Zhao, X.; Sheng, Y.; Lv, H.; Jia, H.; Liu, Q.; Ji, X.; Xiong, R.; Meng, J. Laboratory investigation on road performances of asphalt mixtures using steel slag and granite as aggregate. *Constr. Build. Mater.* **2022**, *315*, 125655. [[CrossRef](#)]
31. Chen, Z.; Xiao, Y.; Pang, L.; Zeng, W.; Wu, S. Experimental assessment of flue gas desulfurization residues and basic oxygen furnace slag on fatigue and moisture resistance of HMA. *Fatigue Fract. Eng. Mater. Struct.* **2014**, *37*, 1242–1253. [[CrossRef](#)]
32. Xue, Y.; Wu, S.; Hou, H.; Zha, J. Experimental investigation of basic oxygen furnace slag used as aggregate in asphalt mixture. *J. Hazard. Mater.* **2006**, *138*, 261–268. [[CrossRef](#)] [[PubMed](#)]
33. Chen, Z.; Xie, J.; Xiao, Y.; Chen, J.; Wu, S. Characteristics of bonding behavior between basic oxygen furnace slag and asphalt binder. *Constr. Build. Mater.* **2014**, *64*, 60–66. [[CrossRef](#)]
34. Coomarasamy, A.; Walzak, T. Effects of moisture on surface chemistry of steel slags and steel slag-asphalt paving mixes. *Transp. Res. Rec.* **1995**, 85–95.
35. Chen, Z.; Wu, S.; Xiao, Y.; Zeng, W.; Yi, M.; Wan, J. Effect of hydration and silicone resin on Basic Oxygen Furnace slag and its asphalt mixture. *J. Clean. Prod.* **2016**, *112*, 392–400. [[CrossRef](#)]
36. Chen, Z.; Leng, Z.; Jiao, Y.; Xu, F.; Lin, J.; Wang, H.; Cai, J.; Zhu, L.; Zhang, Y.; Feng, N.; et al. Innovative use of industrially produced steel slag powders in asphalt mixture to replace mineral fillers. *J. Clean. Prod.* **2022**, *344*, 131124. [[CrossRef](#)]
37. Ma, T.; Zhang, D.; Zhang, Y.; Hong, J. Micromechanical response of aggregate skeleton within asphalt mixture based on virtual simulation of wheel tracking test. *Constr. Build. Mater.* **2016**, *111*, 153–163. [[CrossRef](#)]
38. Tao, G.; Xiao, Y.; Yang, L.; Cui, P.; Kong, D.; Xue, Y. Characteristics of steel slag filler and its influence on rheological properties of asphalt mortar. *Constr. Build. Mater.* **2019**, *201*, 439–446. [[CrossRef](#)]
39. Li, C.; Xiao, Y.; Chen, Z.; Wu, S. Crack resistance of asphalt mixture with steel slag powder. *Emerg. Mater. Res.* **2017**, *6*, 214–218. [[CrossRef](#)]
40. *JTG E42-2005*; Test Methods of Aggregate for Highway Engineering. Ministry of Transport of the People’s Republic of China: Beijing, China, 2005. (In Chinese)
41. *JTG E20-2011*; Standard Test Methods of Bitumen and Bituminous Mixtures for Highway Engineering. Ministry of Transport of the People’s Republic of China: Beijing, China, 2011. (In Chinese)
42. *JTG F40-2004*; Technical Specifications for Construction Highway Asphalt Pavements. Ministry of Transport of the People’s Republic of China: Beijing, China, 2004. (In Chinese)
43. Xie, J.; Chen, J.; Wu, S.; Lin, J.; Wei, W. Performance characteristics of asphalt mixture with basic oxygen furnace slag. *Constr. Build. Mater.* **2013**, *38*, 796–803. [[CrossRef](#)]
44. Qiu, L.J.Z.; Chen, Z.W.; Wang, M.; Zeng, W.B. Effect of Aggregate Morphological Characteristics on the High-Temperature Performance of Steel Slag Based HMA. *Key Eng. Mater.* **2014**, *599*, 19–22. [[CrossRef](#)]
45. Wang, Q.; Yan, P.; Han, S. The influence of steel slag on the hydration of cement during the hydration process of complex binder. *Sci. China Technol. Sci.* **2011**, *54*, 388–394. [[CrossRef](#)]
46. Gorkem, C.; Sengoz, B. Predicting stripping and moisture induced damage of asphalt concrete prepared with polymer modified bitumen and hydrated lime. *Constr. Build. Mater.* **2009**, *23*, 2227–2236. [[CrossRef](#)]
47. Xie, J.; Wu, S.; Lin, J.; Cai, J.; Chen, Z.; Wei, W. Recycling of basic oxygen furnace slag in asphalt mixture: Material characterization & moisture damage investigation. *Constr. Build. Mater.* **2012**, *36*, 467–474. [[CrossRef](#)]

**Disclaimer/Publisher’s Note:** The statements, opinions and data contained in all publications are solely those of the individual author(s) and contributor(s) and not of MDPI and/or the editor(s). MDPI and/or the editor(s) disclaim responsibility for any injury to people or property resulting from any ideas, methods, instructions or products referred to in the content.